A ϕ-FEM approach for finite element simulation of heat transfer : test cases

Michel Duprez*, Vanessa Lleras†, Alexei Lozinski‡, and Killian Vuillemot*

May 2022

We present here some test cases to illustrate the interest of ϕ-FEM, as presented in [1], to solve

$$\partial_t u - \Delta u = f \text{ in } \Omega \times (0,T), \quad u = 0 \text{ on } \Gamma \times (0,T), \quad u(\cdot,0) = u^0 \text{ in } \Omega, \tag{1}$$

where $T > 0$, $\Omega \subset \mathbb{R}^d$, $d = 2, 3$.

1 Simulations

Remark 1.1 (Norms for the simulations)**.** *To illustrate the convergence of the methods with different simulations, we will use manufactured solution, i.e. for a function u_{ex} defined on $\Omega_h \times (0,T)$, we consider*

$$f := u_{ex,t} - \Delta u_{ex}$$

and

$$u_0 := u_{ex}(0).$$

Since it is numerically complex to compute the error on the exact domain Ω, we will use the following formula

$$\frac{\|u_h - u_{ex}\|^2_{L^2(0,T,H^1_0(\Omega_h))}}{\|u\|^2_{L^2(0,T,H^1_0(\Omega_h))}} \approx \frac{\sum_{n=0}^N \Delta t \int_{\Omega_h} |\nabla u_h(.,t_n) - \nabla u(.,t_n)|^2 \mathrm{d}x}{\sum_{n=0}^N \Delta t \int_{\Omega_h} |\nabla u(.,t_n)|^2 \mathrm{d}x},$$

and

$$\frac{\|u_h - u_{ex}\|^2_{L^\infty(0,T,L^2(\Omega_h))}}{\|u_{ex}\|^2_{L^\infty(0,T,L^2(\Omega_h))}} \approx \frac{\max_{n=0,\dots,N} \int_{\Omega_h} (u_h(.,t_n) - u_{ex}(.,t_n))^2 \mathrm{d}x}{\max_{n=0,\dots,N} \int_{\Omega_h} (u_{ex}(.,t_n))^2 \mathrm{d}x}.$$

First test case.

We will now illustrate some interesting properties of ϕ-FEM on a test case where we will consider a manufactured solution. We will use the following example : consider the circle centered at the point $(0.5, 0.5)$ of radius $\frac{\sqrt{2}}{4}$, that means ϕ is defined by $\phi(x,y) = -0.125 + (x-0.5)^2 + (y-0.5)^2$ and we consider the problem with the exact manufactured solution

$$u_{ex}(x,y,t) = \exp(x)\sin(2\pi y)\sin(t),$$

and the boundary condition

$$u^g = u_{ex}(1+\phi).$$

We obtain the figures 1, 2, 3 and 4 that illustrate well the expected convergence orders from theorem [1, Theorem 1]. We also obtained the figures 5 and 6 where we have represented the error and the condition number in relation with the stabilization parameter σ.

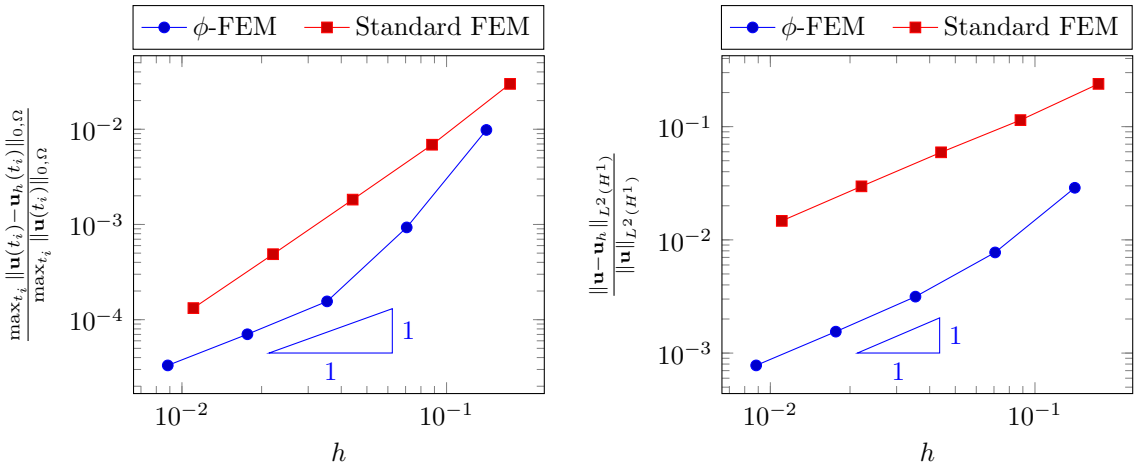

Figure 1: Test case 1; $\Delta t = h$, $\mathbb{P}^1$, $\sigma = 20$. Left: $L^\infty(0,T;L^2(\Omega))$ relative errors. Right: $L^2(0,T;H^1(\Omega))$ relative errors.

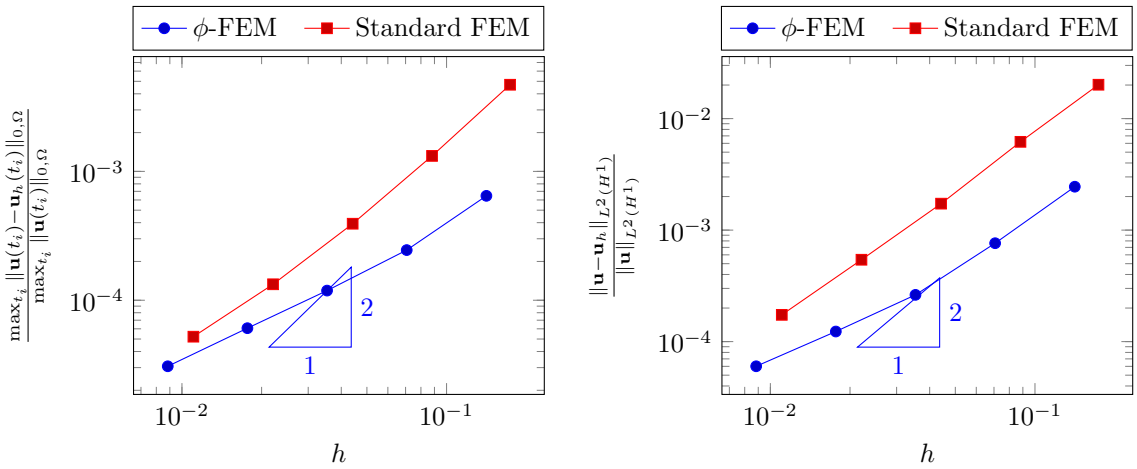

Figure 2: Test case 1: $\Delta t = h$, $\mathbb{P}^2$, $\sigma = 20$. Left: $L^\infty(0,T;L^2(\Omega))$ relative errors. Right: $L^2(0,T;H^1(\Omega))$ relative errors.

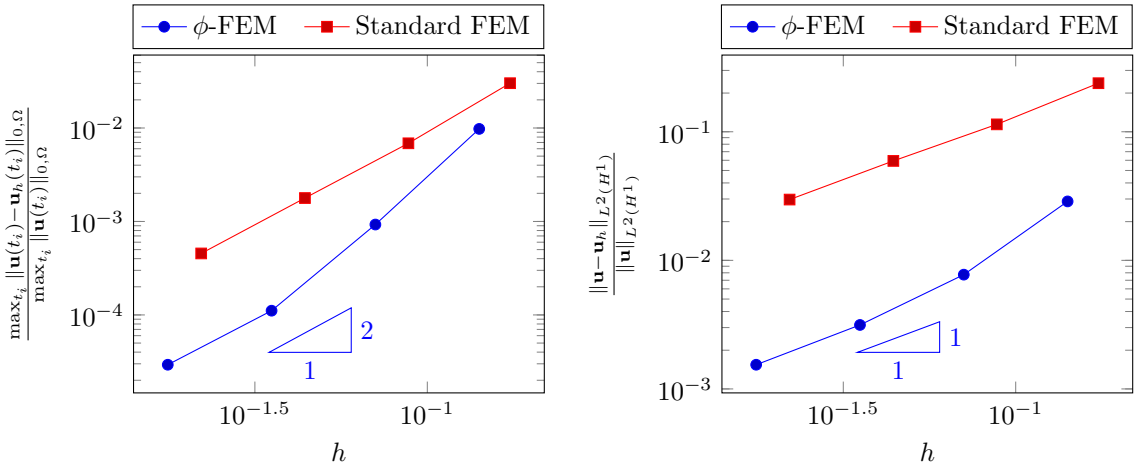

Figure 3: Test case 1: $\Delta t = 10h^2$, $\mathbb{P}^1$. Left: $L^\infty(0,T;L^2(\Omega))$ relative errors. Right: $L^2(0,T;H^1(\Omega))$ relative errors.

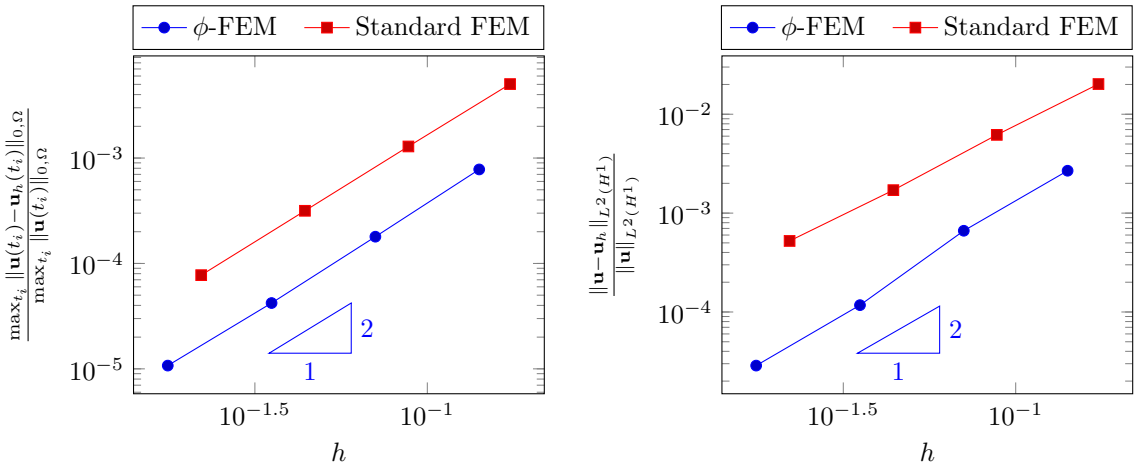

Figure 4: Test case 1: $\Delta t = 10h^2$, $l = 2$. Left: $L^\infty(0,T;L^2(\Omega))$ relative errors. Right: $L^2(0,T;H^1(\Omega))$ relative errors.

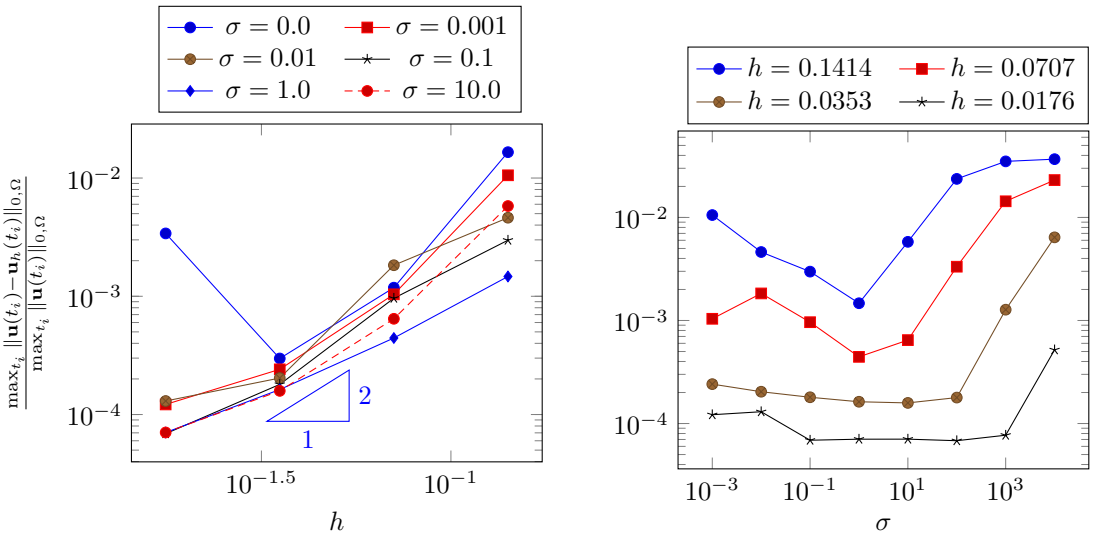

Figure 5: Test case 1: $\Delta t = h$. $L^\infty(0,T;L^2(\Omega))$ relative errors.

We also want to numerically illustrate the evolution of the condition number on the figure 5. To do that, we consider the same case, using a time-step $\Delta t = h$, and we consider different values of σ and h.

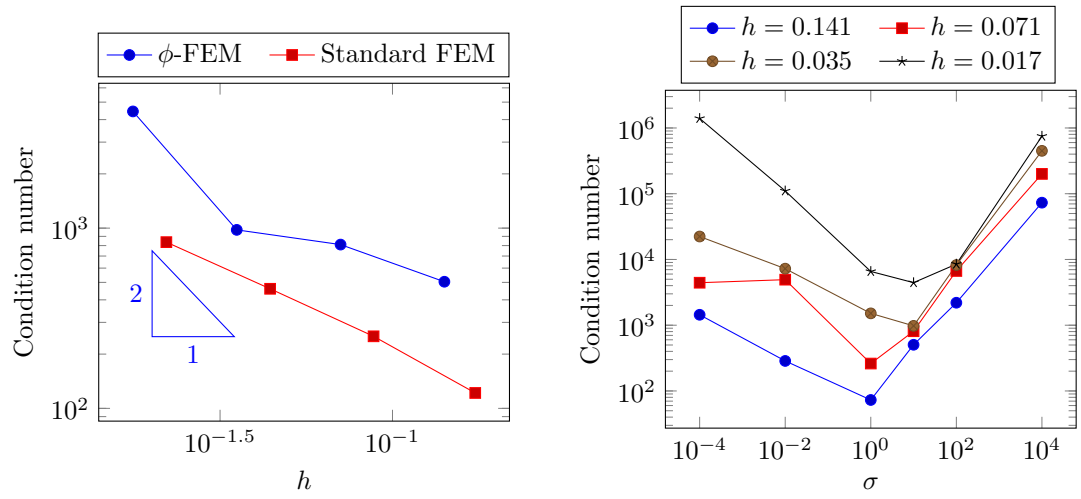

Figure 6: Test case 1: $\Delta t = h$. Condition number. Left : $\sigma = 10$.

Second test case.

We decide to implement a ϕ-FEM scheme using a Crank-Nicolson discretization in time. Recalling that the Crank-Nicolson scheme for the equation (1) is given by

*MIMESIS team, Inria Nancy - Grand Est, MLMS team, Université de Strasbourg, France.
†IMAG, Univ Montpellier, CNRS, Montpellier, France.
‡Laboratoire de Mathématiques de Besançon, UMR CNRS 6623, Université de Bourgogne Franche-Comté, France.

$$\frac{1}{\Delta t}(u^{n+1}-u^n)-\frac{1}{2}\left(\Delta u^{n+1}+\Delta u^n\right)=\frac{1}{2}\left(f(t_{n+1})+f(t_n)\right)\,, \tag{2}$$

we can thus define a ϕ-FEM scheme for this method, given by : find $w_h^n \in V_h^{(l)}$ such that, for all $v_h \in V_h^{(l)}$

$$\begin{aligned}
&\int_{\Omega_h}\frac{\phi_h w_h^{n+1}}{\Delta t}\phi_h v_h+\frac{1}{2}\int_{\Omega_h}\nabla(\phi_h w_h^{n+1})\cdot\nabla(\phi_h v_h)-\frac{1}{2}\int_{\partial\Omega_h}\frac{\partial}{\partial n}(\phi_h w_h^{n+1})\phi_h v_h\\
&\qquad+\frac{1}{2}G_h(\phi_h w_h^{n+1},\phi_h v_h)-\sigma h^2\int_{\Omega_h^\Gamma}\left(\frac{\phi_h w_h^{n+1}}{\Delta t}-\frac{1}{2}\Delta(\phi_h w_h^{n+1})\right)\Delta(\phi_h v_h)\\
&\qquad=\int_{\Omega_h}\frac{\phi_h w_h^{n}}{\Delta t}\phi_h v_h+\int_{\Omega_h}\frac{1}{2}\left(f^{n+1}+f^n\right)\phi_h v_h-\frac{1}{2}G_h(\phi_h w_h^n,\phi_h v_h)\\
&\qquad\quad-\frac{1}{2}\int_{\Omega_h}\nabla(\phi_h w_h^n)\cdot\nabla(\phi_h v_h)+\frac{1}{2}\int_{\partial\Omega_h}\frac{\partial}{\partial n}(\phi_h w_h^n)\cdot\phi_h v_h\\
&\qquad\quad-\sigma h^2\int_{\Omega_h^\Gamma}\frac{1}{2}\left(f^{n+1}+f^n\right)\Delta(\phi_h v_h)-\sigma h^2\int_{\Omega_h^\Gamma}\left(\frac{\phi_h w_h^n}{\Delta t}+\frac{1}{2}\Delta(\phi_h w_h^n)\right)\Delta(\phi_h v_h)\,,
\end{aligned}$$

where

$$G_h(\phi_h w,\phi_h v):=\sigma h\sum_{E\in\mathcal{F}_h^\Gamma}\int_E\left[\frac{\partial}{\partial n}(\phi_h w)\right]\left[\frac{\partial}{\partial n}(\phi_h v)\right]\,.$$

Using this scheme on the previous test case, with the same parameters using $\mathbb{P}^1$ and $\mathbb{P}^2$ finite elements, we get the results on the figures 7 and 8 where we can see the efficiency of ϕ-FEM.

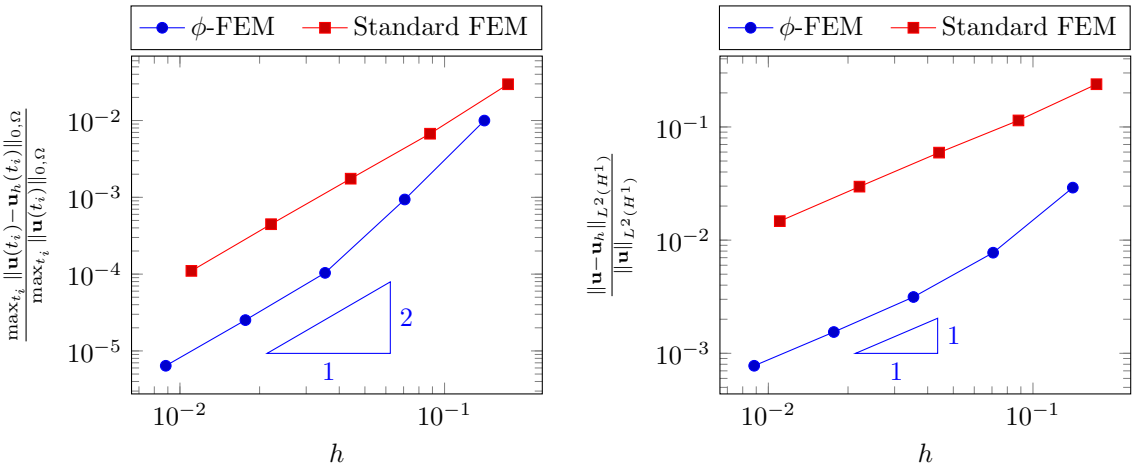

Figure 7: Test case 2: $\Delta t = h$, $\mathbb{P}^1$, $\sigma = 20$. Left: $L^\infty(0,T;L^2(\Omega))$ relative errors. Right: $L^2(0,T;H^1(\Omega))$ relative errors.

Third test case.

Now, let Ω be the rectangle of corners $\left(\frac{2\pi^2}{\pi^2+1},\frac{\pi^3-\pi}{\pi^2+1}\right)$, $(0,\pi)$, $\left(-\frac{2\pi^2}{\pi^2+1},-\frac{\pi^3-\pi}{\pi^2+1}\right)$, $(0,-\pi)$ and $\phi(x,y) = -(y-\pi x-\pi)\times(y+x/pi-\pi)\times(y-\pi x+\pi)\times(y+x/pi+\pi)$.

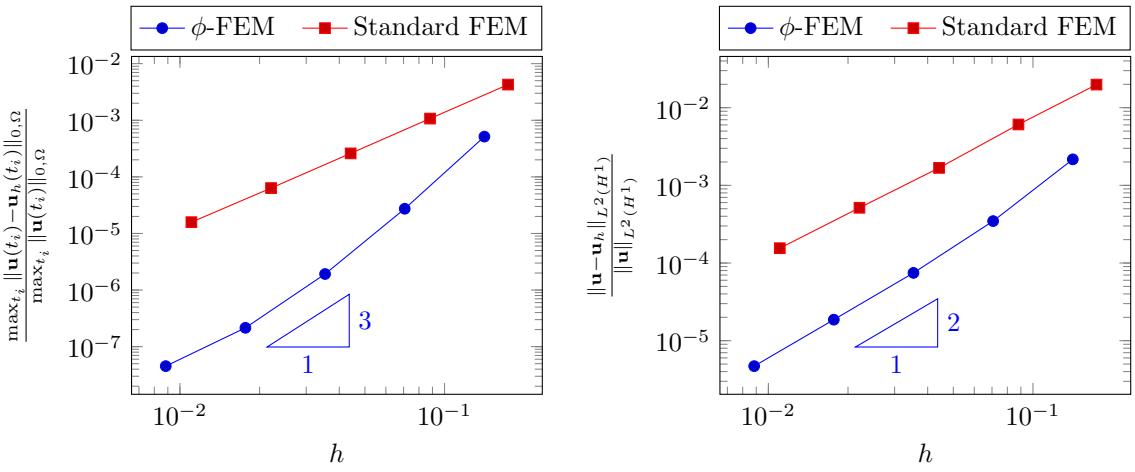

Figure 8: Test case 2: $\Delta t = h$, $\mathbb{P}^2$, $\sigma = 20$. Left: $L^\infty(0,T;L^2(\Omega))$ relative errors. Right: $L^2(0,T;H^1(\Omega))$ relative errors.

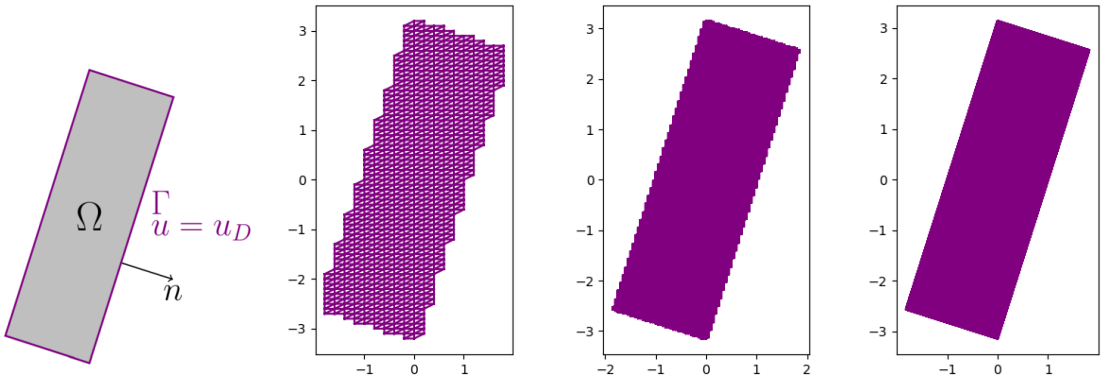

Figure 9: Test case 3. Left : considered situation. Middle : two ϕ-FEM meshes for different iterations. Right : fine mesh, used to solve (3) with standard FEM.

We can try to use ϕ-FEM to solve numerically the problem (3), given by,

$$\begin{cases} u_t - \Delta u = 1 & \text{sur } \Omega \times (0,T) \\ u = \sin(x)\cos(y) & \text{sur } \Gamma \times (0,T) \\ u(\cdot,0) = 2\sin(x)\exp(y) & \text{sur } \Omega\,. \end{cases} \tag{3}$$

To illustrate the situation, we represent Ω and three meshes used to solve : problem, on the figure 9.

To compute the error, we consider here as exact solution the solution given by a standard FEM on the fine mesh from 9.

We then apply the ϕ-FEM scheme defined before, using Implicit Euler to solve the problem (3) and we represent the different errors on the figure 10.

Finally, we also decide to illustrate the evolution in time of the solution given by our ϕ-FEM scheme and of the one given by the standard FEM, on figures 11 and 12. To do that, we consider the last iteration of ϕ-FEM, that implies a cell size $h \approx 0.0279$. Note that to compute the error of ϕ-FEM and to represent the solution, we need to project the solution of the scheme on the standard FEM mesh. Thus, it implies that all the meshes that we consider for the representations are exactly the same.

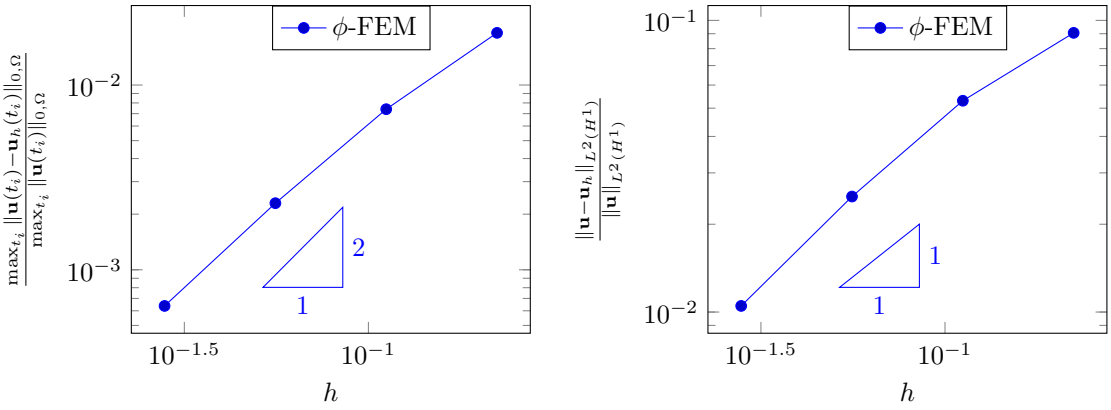

Figure 10: Test case 3; $\Delta t = h$, $\mathbb{P}^1$, $\sigma = 20$. Left: $L^\infty(0,T;L^2(\Omega))$ relative errors. Right: $L^2(0,T;H^1(\Omega))$ relative errors.

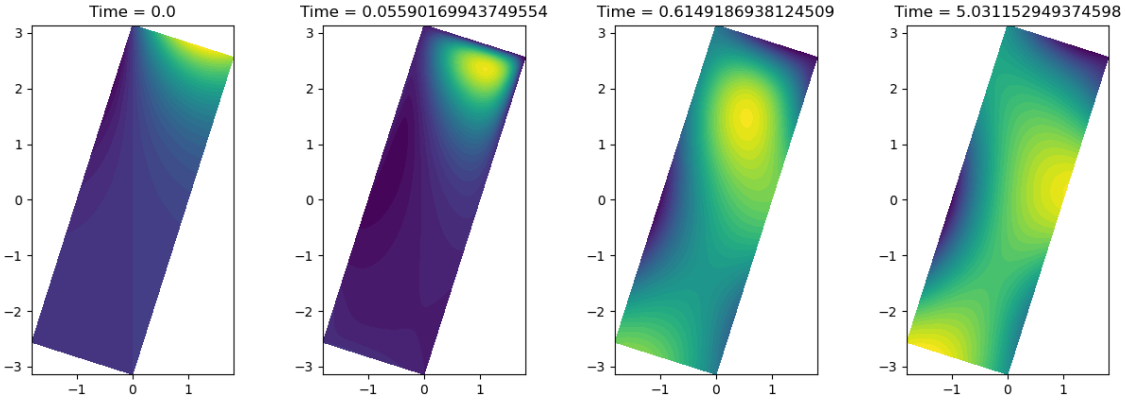

Figure 11: Test case 3. ϕ-FEM solutions, with $\sigma = 20$, $\mathbb{P}^1$ finite elements and $h \approx 0.0279$.

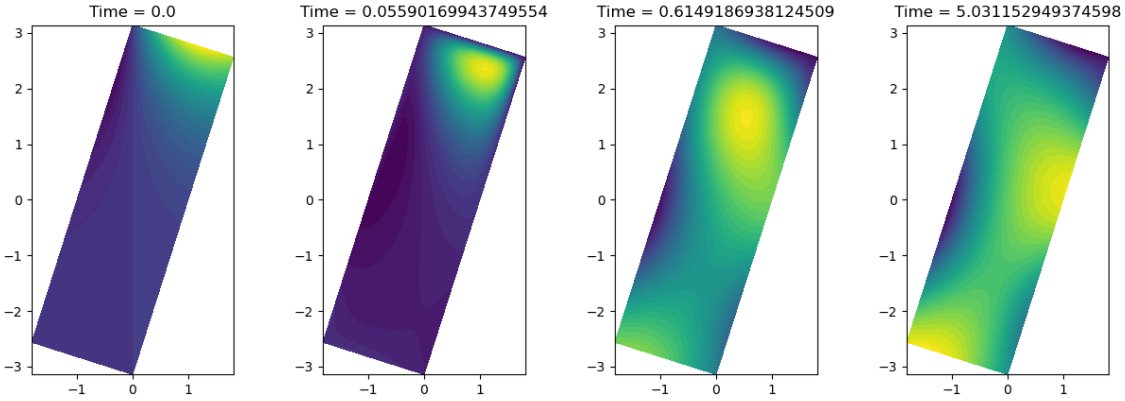

Figure 12: Test case 3. standard FEM solutions, with $\sigma = 20$, $\mathbb{P}^1$ finite elements and $h \approx 0.022$.

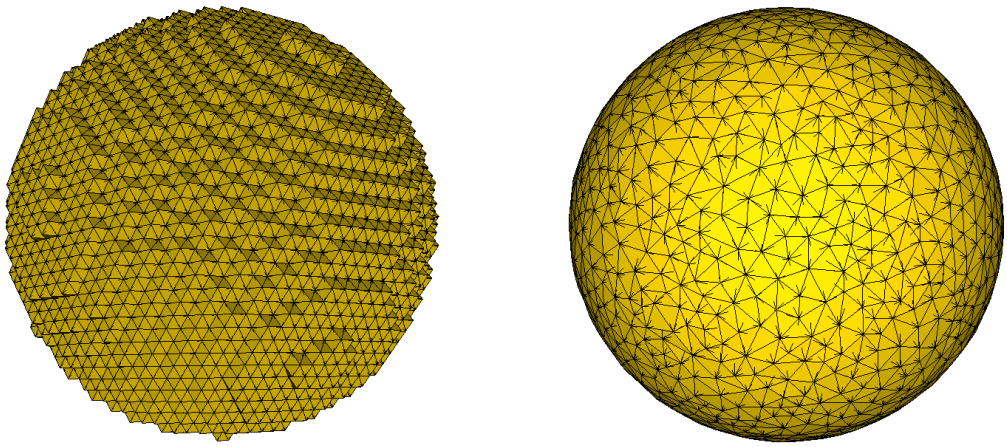

Figure 13: Left : regular mesh used for ϕ-FEM. Right : mesh built for the standard method.

Test case 4 : a 3-dimensional problem

For this test case we are going to consider one more time a manufactured solution to illustrate the convergence of our method to solve a problem in 3 dimensions. For that, we consider a kind of extension of the first test case. We choose to consider this time the sphere centered at the point $(0.5, 0.5, 0.5)$ of radius $\sqrt{2}/4$. Therefore, we define our level-set function ϕ by

$$\phi(x, y, z) = -0.125 + (x - 0.5)^2 + (y - 0.5)^2 + (z - 0.5)^2 \,,$$

and the exact manufactured solution by

$$u_{ex}(t, x, y, z) = \exp(x) \sin(2\pi y) \sin(2\pi z) \sin(t) \,,$$

with the boundary condition

$$u^g = u_{ex}(1 + \phi) \,.$$

The two finest meshes that are considered during the computation are represented on the figure 13, to illustrate the difference between the mesh considered for the standard method and the regular mesh defined using ϕ.

We give the results on the figure 14 where we can remark that even with this type of problems, the convergence orders are numerically verified.

Test case 5 : the case of BDF2

We consider here the same problem as in the first test case. We first write the governing equations that we consider for this method. For this time discretization, the equation

$$u_t - \Delta u = f \,,$$

can be rewritten at the time t^n as

$$u_n - \frac{2}{3}\Delta t \Delta u^n = \frac{2}{3}\Delta t f^n + \frac{4}{3}u^{n-1} - \frac{1}{3}u^{n-2} \,.$$

Since we need the two previous terms u^{n-1} and u^{n-2}, we will first compute u^1 using a Crank-Nicolson scheme as introduced in the second test case.

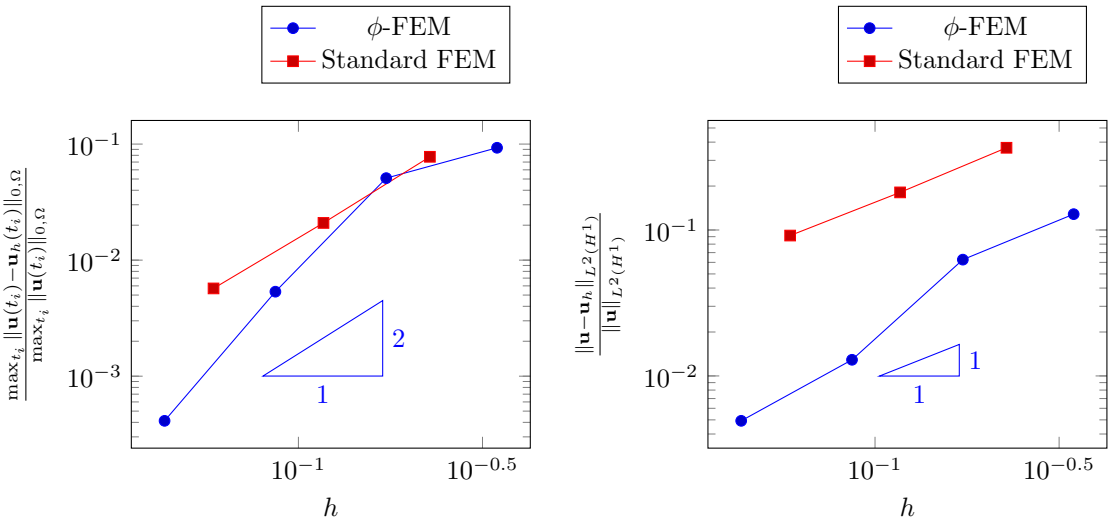

Figure 14: Test case 4: $\Delta t = h$, $\mathbb{P}^1$, $\sigma = 20$. Left: $L^\infty(0,T;L^2(\Omega))$ relative errors. Right: $L^2(0,T;H^1(\Omega))$ relative errors.

Now that we have our discrete equation we can give the corresponding ϕ-FEM scheme that is, find $w_h^n \in V_h^{(l)}$ such that for all $v_h \in V_h^{(l)}$

$$\begin{aligned}\int_{\Omega_h} \phi_h w_h^n \phi_h v_h + \frac{2}{3}\Delta t \int_{\Omega_h} \nabla(\phi_h w_h^n)\cdot\nabla(\phi_h v_h) - \frac{2}{3}\Delta t \int_{\Gamma_h} \partial_n(\phi_h w_h^n)\phi_h v_h + \frac{2}{3}\Delta t G_h(\phi_h w_h^n, \phi_h v_h) \\ - \sigma h^2 \int_{\Omega_h^\Gamma} \left(\phi_h w_h^n - \frac{2}{3}\Delta t \Delta(\phi_h w_h^n)\right)\Delta(\phi_h v_h) = \frac{2}{3}\Delta t \int_{\Omega_h} f^n \phi_h v_h \\ + \frac{4}{3}\int_{\Omega_h} \phi_h w_h^{n-1}\phi_h v_h - \frac{1}{3}\int_{\Omega_h} \phi_h w_h^{n-2}\phi_h v_h \\ - \sigma h^2 \int_{\Omega_h^\Gamma} \left(\frac{2}{3}\Delta t f^n + \frac{4}{3}\phi_h w_h^{n-1} - \frac{1}{3}\phi_h w_h^{n-2}\right)\Delta(\phi_h v_h)\,.\end{aligned}$$

We finally represent the errors obtained using standard FEM and ϕ-FEM on the figure 15, where we solved the same problem as in the first test case.

References

[1] An Immersed Boundary Method by ϕ-FEM approach to solve the heat equation. Michel Duprez, Vanessa Lleras, Alexei Lozinski and Killian Vuillemot. In preparation, 2022.

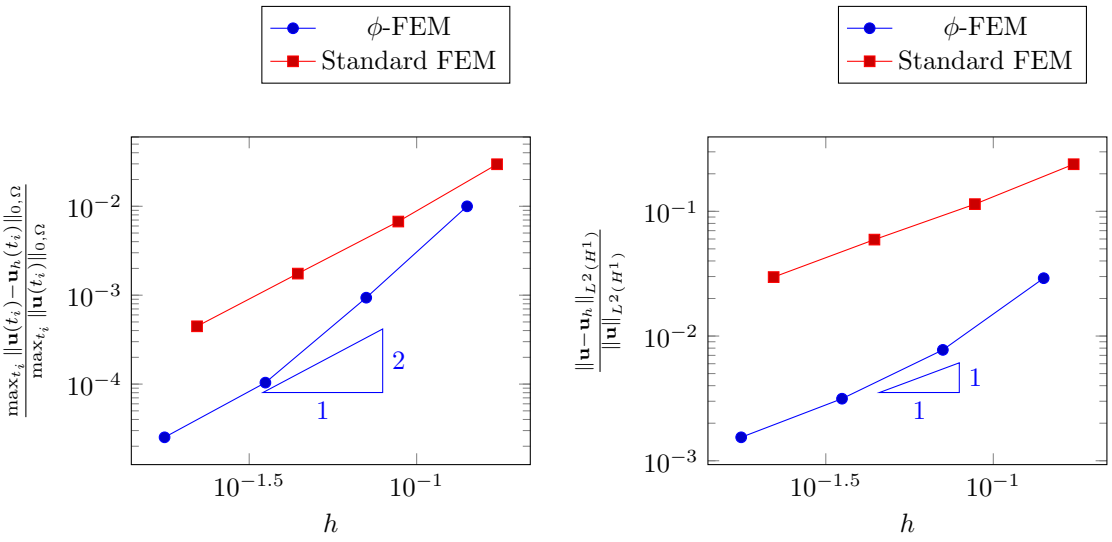

Figure 15: Test case 5: $\Delta t = h$, $\mathbb{P}^1$, $\sigma = 20$. Left: $L^\infty(0,T;L^2(\Omega))$ relative errors. Right: $L^2(0,T;H^1(\Omega))$ relative errors.